Suitability of Explicit Algebraic Stress Models for predicting complex three-dimensional flows

M. Weinmann[*] and Richard D. Sandberg[†]

University of Southampton, Southampton SO17 1BJ, U.K.

For the simulation of complex, three-dimensional turbulent flows within the Reynolds-Averaged Navier-Stokes framework, Explicit-Algebraic-Stress-Models (EASM) constitute an appealing alternative to traditional one- or two-equation turbulence models based on a linear stress-strain relationship. Due to the simplicity and numerical efficiency, two-dimensional EASM formulations are preferred over their more complex three-dimensional counterpart. However, three-dimensional EASM formulations use additional, higher order coupling terms which may have the potential to improve the predicted results for cases with three-dimensional mean flow. The aim of this work is to evaluate the performance of EASM closures for predicting complex three-dimensional flows and to investigate potential differences between two-dimensional and three-dimensional EASM formulations. All models to be investigated are implemented into OpenFOAM and are tested on the flow around an idealized wing-body junction and the flow over an three-dimensional axisymmteric hill. In addition, results are compared to the widely used Kω-SST turbulence model.

I.   Introduction

The Reynolds-Averaged Navier-Stokes (RANS) approach continues to be an important tool for turbulent flow simulations in industrial and engineering environments. At this level of turbulence closure, simulations can be performed for complex geometries with short turnaround times and at moderate computational costs. The closure approximations are typically based on two-equation turbulence models which are used in conjunction with a linear stress-strain relationship. This functional relationship predicts results with fair accuracy for a range of simple and well behaved thin shear flows. In situation where the normal components of the Reynolds stress tensor become important, such as in turbulence driven secondary motion, flow impingement, separation or recirculation to name a few, the linear stress-strain relation fails to produce reliable results. Similar shortcomings exist for flows where body forces and/or 'extra' strain-rates alter the structure of the turbulence in the flow.

The class of turbulence models which circumvents some of these limitations are Differential Reynolds-Stress-Models (DRSM) which solve a transport equation for each of the Reynolds-Stress components. The increased computational effort required by DRSM's coupled with their numerical difficulties for complex three-dimensional flows has lead to the emergence of Explicit-Algebraic-Reynolds-Stress-Models (EASM), where the robustness of traditional two equation models is combined with the improved predictive capabilities of a second moment closure. Even though not all of the features of the underlying DRSM can be retained in the explicit approximation, they constitute a robust alternative to traditional two-equation models providing improved predictive capabilities at slightly increased numerical expense.

In order to reduce the transport equations of DRSM to an algebraic expression, Rodi[1,2] introduced an equilibrium hypothesis which yields an implicit algebraic relation between the Reynolds stress components and the velocity gradients. The set of algebraic equations can be solved by means of representation theory. The most general solution to the algebraic equation consists of an integrity basis with ten independent generators. Pope[3] showed that, in the limit of two-dimensional mean flows, the complete integrity basis can be reduced to three independent generators. Pope was also the first to derive an explicit solution to the implicit algebraic equations of Rodi for two-dimensional mean flows assuming a known ratio of production

---

[*]Post-Graduate Student, School of Engineering Sciences,mw405@soton.ac.uk, AIAA member
[†]Lecturer, School of Engineering Sciences, sandberg@soton.ac.uk, AIAA member

to dissipation. Gatski and Speziale[4] later extended Popes model to three-dimensional mean flows for the general class of models that are tensorially linear in the Reynolds stress anisotropy. Other three-dimensional EASM formulations include those proposed by Taulbee[5] and Wallin and Johannsen.[6]

Gatski and Speziale[4] and Taulbee[5] both apply a linearization of the algebraic equations by retaining the ratio of production to dissipation implicit during the derivation. The assumption of a constant ratio of production to dissipation results in an inconsistent behaviour of the model for flows which are far from equilibrium. This inconsistency may lead to a singular behaviour for large localized strain-rates which in turn results in numerical difficulties. Gatski and Speziale[4] therefore had to apply a regularization procedure to remove the model singularities. Girimaji[7] solves the algebraic equations in their full non-linear form in the limit of two-dimensional mean flows. The ratio of production to dissipation is now governed by a nonlinear equation for which an explicit solution can be obtained for two-dimensional mean flows. Hence, the resulting model becomes a fully explicit and fully consistent approximation to the 'parent' DRSM which is free of singularities. However, for three-dimensional mean flows the nonlinear equation cannot be solved explicitly. Wallin and Johannsen[6] instead suggest to provide an initial guess using the solution of the non-linear equation for two-dimensional flows and to obtain a more accurate solution by using a perturbation solution of the three-dimensional equation.

The range of existing Explicit Algebraic Stress Models derived for three-dimensional mostly use the full integrity basis and, therefore, yield very complex and lengthy expressions for the coefficients of the generators in the integrity basis. In addition, fully explicit solutions are only approximately self consistent for three-dimensional flows. In the limit of two-dimensional mean flow, the EASM formulations reduce to much more compact forms and provide fully explicit and fully consistent solutions. Therefore, it seems very appealing to apply these two-dimensional formulations even for genuinely three-dimensional mean flows. On the other hand, the additional generators appearing in three-dimensional EASM formulations constitute additional higher order nonlinear coupling terms which may significantly improve the performance of the EASM in general three-dimensional flows.

The aim of this work is to evaluate the performance of Explicit-Algebraic-Stress-Models for predicting complex three-dimensional flows and to investigate the suitability of simplified, two-dimensional EASM formulations compared to EASM formulations derived for three-dimensional mean flows. In addition, the impact of a non-linear stress-strain relationship is evaluated by comparing the results to the Kω-SST model. Simulations are performed for two different test cases which both exhibit strongly three-dimensional mean flow. The test cases considered are the flow around an idealized wing-body junction, and the flow around a three-dimensional axisymmteric hill. The performance of the EASM turbulence models is evaluated by comparing to experimental data or highly resolved LES/DNS data.

The paper is organized as follows: First, the constitutive relations used in this study are briefly summarized. Section III discusses the computational approach. In Section IV, the correct implementation of all models used in this study is verified by performing simulations for a fully developed turbulent channel flow. Then, the test cases are introduced in detail and the results are presented and discussed. In the final section, the most important results are summarized and the conclusions are highlighted.

II. Constitutive Relations

In this section the constitutive relations of the EASM formulations used in this work are summarized. A detailed derivation and the explicit solution for a general quasi-linear Algebraic-DRSM can be found in reference.[6]

The Reynolds stress tensor in an EASM formulation constitutes a non-linear stress-strain relationship which can be written in the following form

$$\overline{u_i' u_j'} = \frac{2}{3} K \delta_{ij} - 2\nu_T S_{ij}^* + K a_{ij}^{ex}, \tag{1}$$

where $S_{ij}^* = \frac{1}{2} \left(\frac{\partial U_i}{\partial x_j} + \frac{\partial U_j}{\partial x_i} \right)$ is the strain-rate tensor and a_{ij}^{ex} is an extra-anisotropy tensor which introduces 'extra' anisotropy in addition to the anisotropy resulting form the mean flow S_{ij}^*.

For three-dimensional mean flow the extra anisotropy tensor is given as

$$
\begin{aligned}
a_{ij}^{ex} = & \ \beta_2 \left(\boldsymbol{S}^2 - \frac{1}{3} II_S \boldsymbol{I} \right) + \beta_3 \left(\boldsymbol{\Omega}^2 - \frac{1}{3} II_\Omega \boldsymbol{I} \right) + \beta_4 \left(\boldsymbol{S\Omega} - \boldsymbol{\Omega S} \right) \\
& + \beta_5 \left(\boldsymbol{S}^2 \boldsymbol{\Omega} - \boldsymbol{\Omega S}^2 \right) + \beta_6 \left(\boldsymbol{S\Omega}^2 + \boldsymbol{\Omega}^2 \boldsymbol{S} - II_\Omega \boldsymbol{S} - \frac{2}{3} IV \boldsymbol{I} \right) \\
& + \beta_7 \left(\boldsymbol{S}^2 \boldsymbol{\Omega}^2 + \boldsymbol{\Omega}^2 \boldsymbol{S}^2 - \frac{2}{3} V \boldsymbol{I} \right) + \beta_8 \left(\boldsymbol{S\Omega S}^2 - \boldsymbol{S}^2 \boldsymbol{\Omega S} \right) \\
& + \beta_9 \left(\boldsymbol{\Omega S\Omega}^2 - \boldsymbol{\Omega}^2 \boldsymbol{S\Omega} \right),
\end{aligned}
\tag{2}
$$

with the invariants

$$
II_S = tr \left\{ \boldsymbol{S}^2 \right\}, \quad II_\Omega = tr \left\{ \boldsymbol{\Omega}^2 \right\}, \quad III = tr \left\{ \boldsymbol{S}^3 \right\},
\tag{3}
$$

$$
IV = tr \left\{ \boldsymbol{S\Omega}^2 \right\}, \quad V = tr \left\{ \boldsymbol{S}^2 \boldsymbol{\Omega}^2 \right\},
\tag{4}
$$

where $\boldsymbol{S}$ and $\boldsymbol{\Omega}$ are the normalized mean strain and rotation-rate tensors

$$
\boldsymbol{S} = S_{ij} = \tau S_{ij}^*, \quad \boldsymbol{\Omega} = \Omega_{ij} = \frac{\tau}{2} \left(\frac{\partial U_i}{\partial x_j} - \frac{\partial U_j}{\partial x_i} \right),
\tag{5}
$$

respectively. The turbulent time scale is limited by the viscous timescale and is given by

$$
\tau = max \left(\frac{1}{0.09\omega}, 20 \sqrt{\frac{\mu}{\rho \omega k}} \right).
\tag{6}
$$

The β_i coefficients for **three-dimensional** mean flow are given as

$$
\begin{aligned}
\beta_1 &= -0.5 A_1 N \left(30 A_2 IV - 21 N II_\Omega - 2 A_2^3 III + 6 N^3 - 3 A_2^2 II_S N \right) / Q \\
\beta_2 &= -A_1 A_2 \left(6 A_2 IV + 12 N II_\Omega + 2 A_2^3 III - 6 N^3 + 3 A_2^2 II_S N \right) / Q \\
\beta_3 &= -3 A_1 \left(2 A_2^2 III + 3 N A_2 II_S + 6 IV \right) / Q \\
\beta_4 &= -A_1 \left(2 A_2^3 III + 3 A_2^2 N II_S + 6 A_2 IV - 6 N II_\Omega + 3 N^3 \right) / Q \\
\beta_5 &= 9 A_1 A_2 N^2 / Q, \quad \beta_6 = -9 A_1 N^2 / Q, \quad \beta_7 = 18 A_1 A_2 N / Q \\
\beta_8 &= 9 A_1 A_2^2 N / Q, \quad \beta_9 = 9 A_1 N / Q,
\end{aligned}
\tag{7}
$$

where

$$
\begin{aligned}
Q = & \ 3 N^5 + \left(-15/2 II_\Omega - 7/2 A_2^2 II_S \right) N^3 + \left(21 A_2 IV - A_2^3 III \right) N^2 \\
& + \left(3 II_\Omega^2 - 8 II_S II_\Omega A_2^2 + 24 A_2^2 V + A_2^4 II_S^2 \right) N + \frac{2}{3} A_2^5 II_S III \\
& + 2 A_2^3 IV II_S - 2 A_2^3 II_\Omega A_2 II_\Omega.
\end{aligned}
\tag{8}
$$

It is now evident, that the fully three-dimensional EASM approximation yields a large number of additional numerical operations which need to be performed compared with linear two-equation models. The β_i coefficients for **two-dimensional** mean flow are given as

$$
\beta_1 = -A_1 N / Q, \quad \beta_2 = 2 A_1 A_2 / Q, \quad \beta_4 = -A_1 / Q, \quad \beta_3 = \beta_5 = \beta_6 = \beta_7 = \beta_8 = \beta_9 = 0,
\tag{9}
$$

where

$$
Q = N^2 - 2 II_\Omega - \frac{2}{3} A_2^2 II_S.
\tag{10}
$$

Hence, the two-dimensional EASM formulation requires only the evaluation of two extra generators compared to a linear formulation. The compactness and moderate additional numerical expense makes the 2D-EASM formulation very appealing.

Wallin and Johannsen[6] suggest to use a modified version of the linear pressure-strain model of Launder _et al._[8] This modification results in a simplified form of the Algebraic-DRSM and consequently in reduced

American Institute of Aeronautics and Astronautics

complexity for the EASM approximation. Even though the resulting model is more compact, it is achieved at the expense of the predictive performance, i.e. it cannot predict anisotropy of the third normal component. In this study the two and three-dimensional EASM formulations are therefore based on the linear pressure-strain model of Speziale *et al.*[9] which is believed to be favourable in complex three-dimensional flows. The coefficients A_i are directly determined from the model of Speziale *et al.*[9] and are given as

$$A_1 = 1.22, \quad A_2 = 0.47, \quad A_3 = 0.88, \quad A_4 = 2.37.$$

The variable N appearing in equation (7)-(10) corresponds to the ratio of production to dissipation and is governed by a non-linear relation. For two-dimensional flows the non-linear equation has an explicit solution which is given by

$$N = \begin{cases} \frac{A_3}{3} + \left(P_1 + \sqrt{P_2}\right)^{1/3} + \left(P_1 - \sqrt{P_2}\right)^{1/3} & , P_2 \geq 0 \\ \frac{A_3}{3} + 2 \left(P_1^2 - P_2\right)^{1/6} \cos\left[\frac{1}{3} \arccos\left(\frac{P_1}{\sqrt{P_1^2 - P_2}}\right)\right] & , P_2 < 0 \end{cases} \tag{11}$$

with

$$P_1 = \left(\frac{A_3^2}{27} + \left(\frac{A_1 A_4}{6} - \frac{2}{9} A_2^2\right) II_S - \frac{2}{3} II_\Omega\right) A_3, \tag{12}$$

$$P_2 = P_1^2 - \left(\frac{A_3^2}{9} + \left(\frac{A_1 A_4}{6} + \frac{2}{9} A_2^2\right) II_S + \frac{2}{3} II_\Omega\right)^3. \tag{13}$$

For the three-dimensional mean flow approximation no explicit solution can be obtained for the production to dissipation ratio. Instead, here the three-dimensional solution is approximated by the solution for two-dimensional mean flow. Finally, the relation for the turbulent viscosity is

$$\nu_T = -\frac{1}{2} \left(\beta_1 + II_\Omega \beta_6\right) k\tau. \tag{14}$$

The relations above must be supplemented by a transport equation for the turbulent velocity scale and a transport equation for the turbulent length scale. The velocity scale is determined from a transport equation for the turbulent kinetic energy K. Many previous studies have independently demonstrated the importance of the length scale equation in the framework of two-equation[10, 11] and second moment closure modeling.[12] Due to the inability of the standard dissipation-rate equation to produce correct length scales in adverse pressure gradient flows, the length scale equation used in this work is based on the formulation proposed by Menter,[13] where the ω-equation is used in the near wall region and blended with the ϵ-equation in the wake region of attached boundary layers. The blending enables improved predictions for adverse pressure gradient flows and avoids the spurious sensitivity of the specific-dissipation rate equation to free-stream values. Note that neither the EASM constitutive relations nor the transport equations for the turbulent scales include modifications for direct integration to solid boundaries. This will only affect the predictions of the turbulent quantities close to wall, the skin friction and mean velocity predictions are unaffected, as will be shown in section IV.A.

The transport equations for the turbulent kinetic energy K and the specific dissipation rate ω take the following form

$$\frac{DK}{Dt} = P_K - \beta^* K \omega + \frac{\partial}{\partial x_j} \left[\left(\nu + \sigma_K \nu_T\right) \frac{\partial K}{\partial x_j}\right], \tag{15}$$

$$\frac{D\omega}{Dt} = \gamma \frac{\omega}{K} P_K - \beta \omega^2 + \frac{\partial}{\partial x_j} \left[\left(\nu + \sigma_\omega \nu_T\right) \frac{\partial \omega}{\partial x_j}\right] + \frac{\sigma_d}{\omega} max\left(CD_{K\omega}, 0\right), \tag{16}$$

where $P_K = -\overline{u_i' u_j'} \frac{\partial U_i}{\partial x_j}$ is the production of turbulent kinetic energy and $CD_{K\omega} = \frac{\partial K}{\partial x_j} \frac{\partial \omega}{\partial x_j}$ is a turbulent cross-diffusion term, arising from the formal transformation of the equation for the dissipation rate ϵ to a form based on the specific dissipation rate ω. The closure coefficients are obtained by blending the respective sets of coefficients from the ω and ϵ formulations

$$\phi = F_1 \phi_1 + (1 - F_1) \phi_2 \tag{17}$$

The blending function F_1 used in this study follows the proposal of Hellsten[14]

$$F_1 = \tanh\left(1.5\Gamma^4\right), \tag{18}$$

with

$$\Gamma = min\left[\max\left(\Gamma_1, \Gamma_2\right), \Gamma_3\right], \tag{19}$$

where

$$\Gamma_1 = \frac{\sqrt{K}}{\beta^*\omega y}, \quad \Gamma_2 = \frac{500\nu}{\omega y^2}, \quad \Gamma_3 = \frac{20K}{max\left[y^2 CD_{K\omega}/\omega, 200K_\infty\right]}. \tag{20}$$

The closure coefficients are optimized for the EASM constitutive relations and are obtained from Hellsten[14]

Set 1: $\quad \gamma_1 = 0.518, \quad \beta_1 = 0.0747, \quad \sigma_{K_1} = 1.1, \quad \sigma_{\omega_1} = 0.53, \quad \sigma_{d_1} = 1.0.$

Set 2: $\quad \gamma_2 = 0.440, \quad \beta_2 = 0.0828, \quad \sigma_{K_2} = 1.1, \quad \sigma_{\omega_2} = 1.00, \quad \sigma_{d_2} = 0.4.$

III.   Methodology

All models to be tested here are implemented into the open source finite volume code OpenFOAM.[15] The convective fluxes are discretized using a second order accurate TVD conformal central differencing scheme. The viscous terms use a second-order central differencing scheme. Steady state results are obtained using the SIMPLE pressure correction algorithm. The convergence is assessed by monitoring flow field variables at more than five locations in important regions of the flow field. The simulations were considered to be converged if the change of the flow field is clearly less than 1% over a few hundred iterations.

IV.   Results

Before the results will be discussed, the stability characteristics of the EASM formulations and their additional numerical expense over a linear two-equation model will be briefly discussed. In terms of stability of the simulations, no significant change in the stability characteristics was observed. The two-dimensional EASM was run with exactly the same solver settings as the $K\omega$-SST model. For the three-dimensional EASM formulation the underrelaxation was decreased by 0.1 in order to achieve convergence. The computational expense of each model was evaluated by considering the average time it takes to perform one iteration using the same solver settings. The last 1000 iterations before convergence were used to calculate the average time for one iteration. It was found that the 2D-EASM is only 6% more expensive and the 3D-EASM is found to be almost twice (80%) as expensive compared to the linear $K\omega$-SST. The large computational time of the 3D-EASM could possibly be reduced by further optimization of the current implementaion.

A.   Planar Channel Flow

In order to verify the correct implementation of the turbulence models used in this study, first a fully developed turbulent channel flow is considered. The flow under consideration has a Reynolds number of $Re_\tau = 590$, based on the skin friction velocity u_τ and the channel half-width $H/2$. DNS[16] results are used to assess the performance of the EASM turbulence models. As a reference, the results of the $k\omega$-SST turbulence model are also included. The computational grid employed has a first wall-normal grid-spacing of $y^+ \approx 0.4$ and 120 cells in the wall normal direction. Figure 1 shows the mean velocity, Reynolds stress components and normal components of the anisotropy tensor $a_{ij} = \tau_{ij}/K - 2/3\delta_{ij}$ in the channel. All variables are normalized using the skin-frictions velocity u_τ.

The mean velocity profile predicted by the $K\omega$-SST and both 2D/3D-EASM formulations is very similar. All models are capable of reproducing the correct log-law behaviour without the need for additional corrections when integrated through the viscous sublayer. Considering the predicted Reynolds stress and stress-anisotropy profiles, it is evident that both the two and three-dimensional EASM models are superior compared to the $K\omega$-SST which uses a linear stress-strain relationship. The nonlinear EASM models predict the Reynolds stress components and anisotropies in the log-layer very well, whereas the linear models cannot predict any stress-anisotropy for this case. The figures also highlight the deficiency of the current EASM constitutive relations to predict the highly anisotropic flow close to the wall ($y^+ < 100$). This is due to the lack of adequate modifications of the quasi-homogeneous pressure strain model and the high-Reynolds number form of the transport equations for the turbulence quantities. Finally, the difference between the 2D-EASM and 3D-EASM are, as one would expect, vanishing in this case.
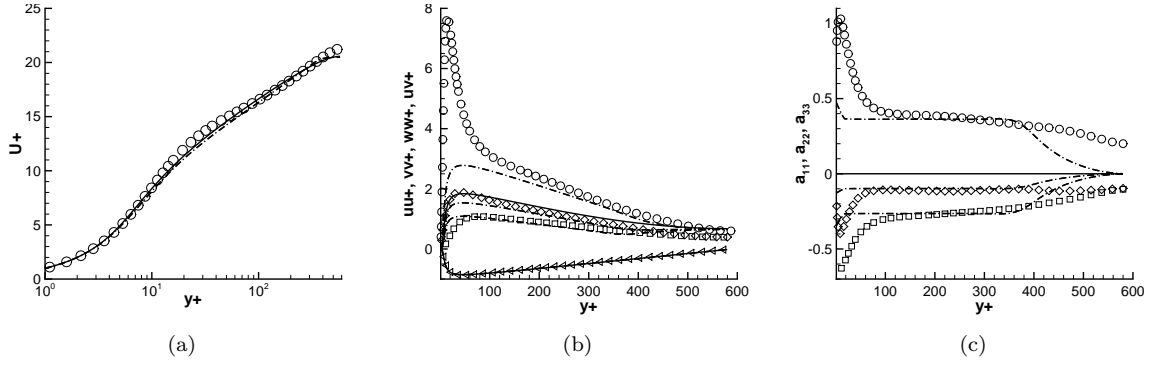
Figure 1. Normalized velocity U^+ (a) , normal and shear-stress profiles (b): uu^+ (○); vv^+ (□) ; ww^+ (◇); uv^+ (◁), stress-anisotropy profiles (c): a_{11} (○); a_{22} (□) ; a_{33} (◇). (—) Kω-SST, ($-\cdot-$) EASM 2D, (- - -) EASM 3D.

B. Flow around an idealized wing-body junction

The idealized wing-body junction as shown in figure 2 consists of a NACA0020 airfoil with a modified 3:2 semi-elliptical nose, which is mounted on a flat plate. The Reynolds number of the configuration under consideration is $Re_T = 115,000$, based on the thickness of the wing T. The wing is approached by a turbulent boundary layer which separates under the action of an adverse pressure gradient from the body wall, forming one or more recirculation regions in front of the base of the wing. The spanwise pressure gradient reorients the vortex generated in front of the wing such that its associated vorticity becomes realigned with the direction of the approaching flow. As a consequence of the realignment, the flow becomes highly skewed and highly three-dimensional in the corner, as discussed in reference.[17] The vortical structure of the recirculation region in front of the wing stretches around the wing and results in a typical three-dimensional horseshoe vortex structure which induces a strong transverse circulation in the corner. An accurate prediction of the stagnation region at the base of the wing and, hence, the origin of the horseshoe vortex is crucial to the outcome of the simulation since an erroneous prediction of this region will influence the downstream development of the vortex. The flow in the separation and stagnation region upstream of the wing exhibits effects like strong streamline curvature and strong normal straining; physical phenomena that are usually not represented satisfactorily by models based on a linear-stress strain relationship. Simpson[18] argues that the turbulence production by normal stress components is equally important to production by shear stress and, hence, the normal stress components contribute to the mean flow behaviour. Therefore, anisotropy resolving turbulence closures are expected to be superior, at least from a theoretical point of view, in capturing the flow upstream of the wing.

Simulations are performed on a grid with 2.3 million cells where particular attention is payed to the adequate resolution of the near wall region. The average first wall normal grid point is located at $y^+ \approx 0.5$

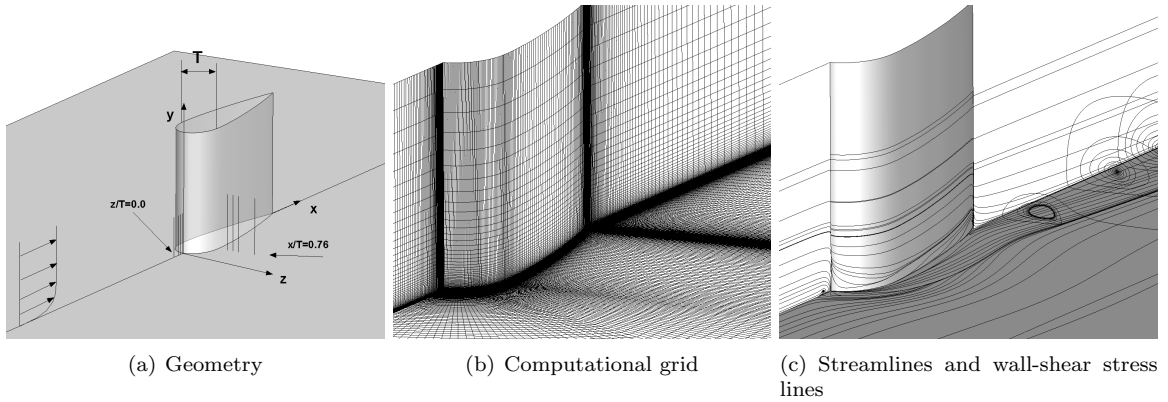(a) Geometry (b) Computational grid (c) Streamlines and wall-shear stress lines

Figure 2. Idealized wing-body junction

and the maximum value is $y^+ \approx 0.9$. Since the geometry is symmetric only half of the domain is modeled. The boundary conditions are a symmetry boundary condition at $z/T = 0$, outflow boundary condition with zero normal gradient at $x/T = 10$, no-slip boundary condition for the wing and the body wall and symmetry boundary conditions at $z/T = 9.5$ and $y/T = 3$. Appropriate inflow conditions at $x/T = -18.24$ are determined from a precursor simulation, where the inflow profile for the velocity and turbulence quantities is obtained by matching the profiles to experimental data.[19]

The simulations are compared with experimental data[19] at different stations in the flow field. The stations include the symmetry plane $z/T = 0$ in the region upstream of wing, and the cross section at maximum chord thickness with $x/T = 0.76$. Figure 3 presents contour plots for the stream-wise velocity U/U_{ref}, the Reynolds-stress components $\overline{uu}/U_{ref}^2$, $\overline{vv}/U_{ref}^2$, $\overline{uv}/U_{ref}^2$ and the turbulent kinetic energy K/U_{ref}^2. Since the component $\overline{ww}/U_{ref}^2$ has not been measured, the turbulent kinetic energy is approximated using the relation $\overline{ww} = 0.5\,(\overline{uu} + \overline{vv})$.[17] The contour plots are supported by figure 4 which presents profiles at four stations in the symmetry plane and allows for a more quantitative comparison.

The experimental data show a separation location at $x/T \approx -0.35$. This is well reproduced by the Kω-SST, which is known for the good response in adverse pressure gradient flows. The 2D and 3D EASM models predict slightly too early separation at about $x/T \approx -0.4$. As a consequence, the Kω-SST model also predicts the vortex core slightly better than the EASM models. It is noted that the EASM formulations incorporate a non-constant value for the constant C_μ, which similarly to the shear-stress limiter in the Kω-SST model, prevents an excessive over prediction of the shear-stress in non-equilibrium flows. Both the 2D and 3D EASM are clearly superior in predicting the streamwise U/U_{ref} and wall normal V/U_{ref} velocity profiles, see figure 4. The EASM models predict the intensity of the reverse flow in close agreement with experimental data, whereas the Kω-SST shows a considerable departure from experimental data. Note that the too weak reverse flow observed here is in contradiction to observation in reference,[17] where the reverse flow was overpredicted. A small difference in the predictions of the mean velocity field between the 2D and 3D-EASM is found, however, the difference is mostly vanishingly small. Therefore, the three-dimensional EASM formulation does not offer any significant advantages.

Overall, the predictions of the turbulence quantities is not as satisfying as the predictions of the mean flow quantities. The turbulence quantities at the first station upstream of the separation location ($x/T = -0.461$) are better predicted by the EASM models using the non-linear stress strain relationship. The improvements can mainly be attributed to the ability of the non-linear EASM models to resolve extra stress-anisotropy, which the Kω-SST cannot. Nevertheless, none of the models investigated is able to adequately capture the strong increase in shear stress inside the vortex at the station $x/T = -0.251$. Similarly, none of the models is able to predict the strong enhancement of the turbulent intensity in the highly sheared region. Even though the non-linear EASM closures predict the normal-stress components and the turbulent kinetic energy somewhat better, the agreements with experimental data inside the vortex is not satisfying. It is interesting to note that, despite the inaccurate prediction of the shear and normal-stress components, the mean velocity profile of both the 2D/3D-EASM are well predicted and are clearly superior to the predictions of the Kω-SST. Figure 3 clearly illustrates the strong damping of the turbulence quantities in the region between the vortex core and the leading edge of the wing where the flow impinges on the body. The strong damping in this region, particularly of the wall normal fluctuations $\overline{vv}/U_{ref}$ very close to the wall is not adequately reproduced by any of the models investigated here (see figure 4 (d), station $x/T = -0.05$). All models significantly overpredict the wall normal turbulent intensity. The traditional way to include the near wall damping into the framework of two-equation models is to introduce ad hoc damping functions which account for both the inviscid wall blockage and the effect of viscosity on the turbulent fluctuations. The turbulence models used in this study do not include any damping functions. These damping functions are completely empirical and are based on quantities which traditionally involve a measure of the viscosity. Even if damping functions were introduced in the current model formulation, the use of viscosity dependent damping functions is based on the wrong rationale, and the success for predicting the correct damping in this case cannot be guaranteed. The need for damping functions originates mainly from the inviscid wall blockage effect and the associated damping of the wall normal fluctuations. Durbin[20] was the first to acknowledge this issue and developed a model which solves a transport equation for the wall normal fluctuations $\overline{v^2}$. In this model formulation, the near wall damping is naturally included. The simulations of Parneix $et\ al.$[21] show that the $\overline{v^2} - f$ reproduces the damping in the impingement region very well.
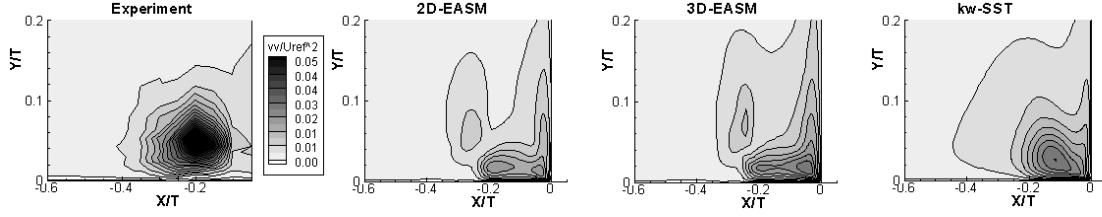
In the region upstream of the wing ($x/T = -0.05$), the difference between the predictions of the turbulence quantities from the 2D and 3D EASM models becomes more pronounced. For all other stations upstream, the
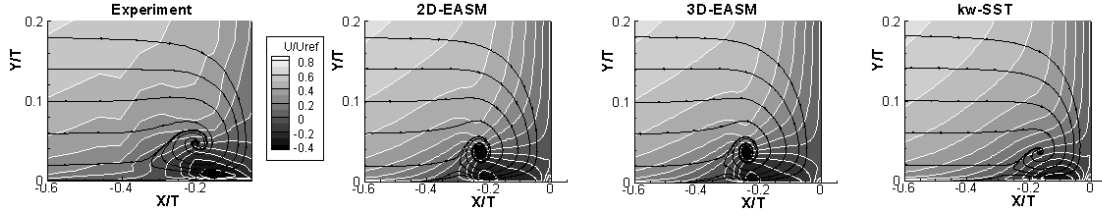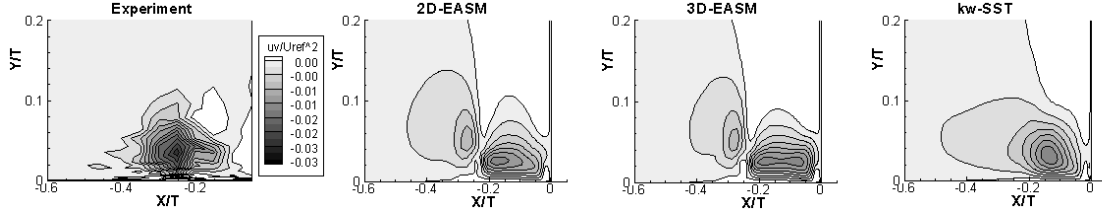
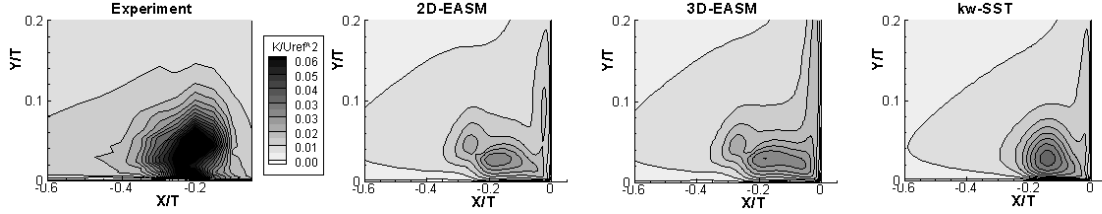(a) normalized velocity U/U_{ref} contour including streamlines
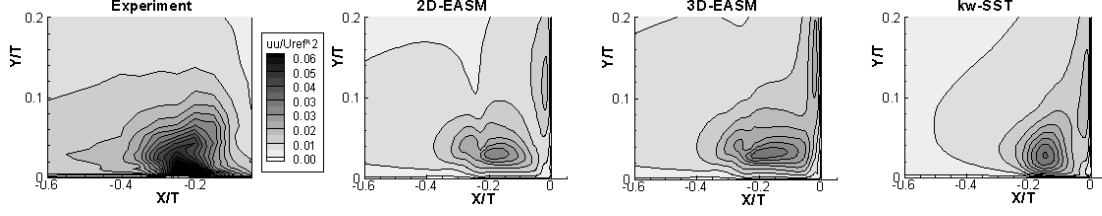
(b) normal stress $\overline{uu}/U_{ref}^2$

(c) normal stress $\overline{vv}/U_{ref}^2$

(d) shear-stress $\overline{uv}/U_{ref}^2$

(e) turbulent kinetic energy K/U_{ref}^2

Figure 3. Contour plots for the symmetry plane at $z/T = 0$.

difference is less pronounced and both EASM versions predict the same trend with only a minor offset in the peak values, indicating an insignificant contribution of the higher order terms in this region. At the station $x/T = -0.05$, the three-dimensional EASM formulation gives the poorest agreement with experimental data and strongly overpredicts the peaks in the turbulence quantities close to the wall.

Figure 5 shows the results for the streamwise velocity U/U_{ref}, transverse velocity W/U_{ref} and the Reynolds-stress components $\overline{uu}/U_{ref}^2$, $\overline{vv}/U_{ref}^2$, $\overline{uv}/U_{ref}^2$, and the turbulent kinetic energy K/U_{ref}^2 at the cross section where the wing reaches the maximum thickness ($x/T = 0.76$). At this plane the vorticity of the vortex has roughly realigned with the downstream flow. As expected, the quality of the predictions in the regions where the horseshoe vortex is formed determines the predictions farther downstream. It is evident
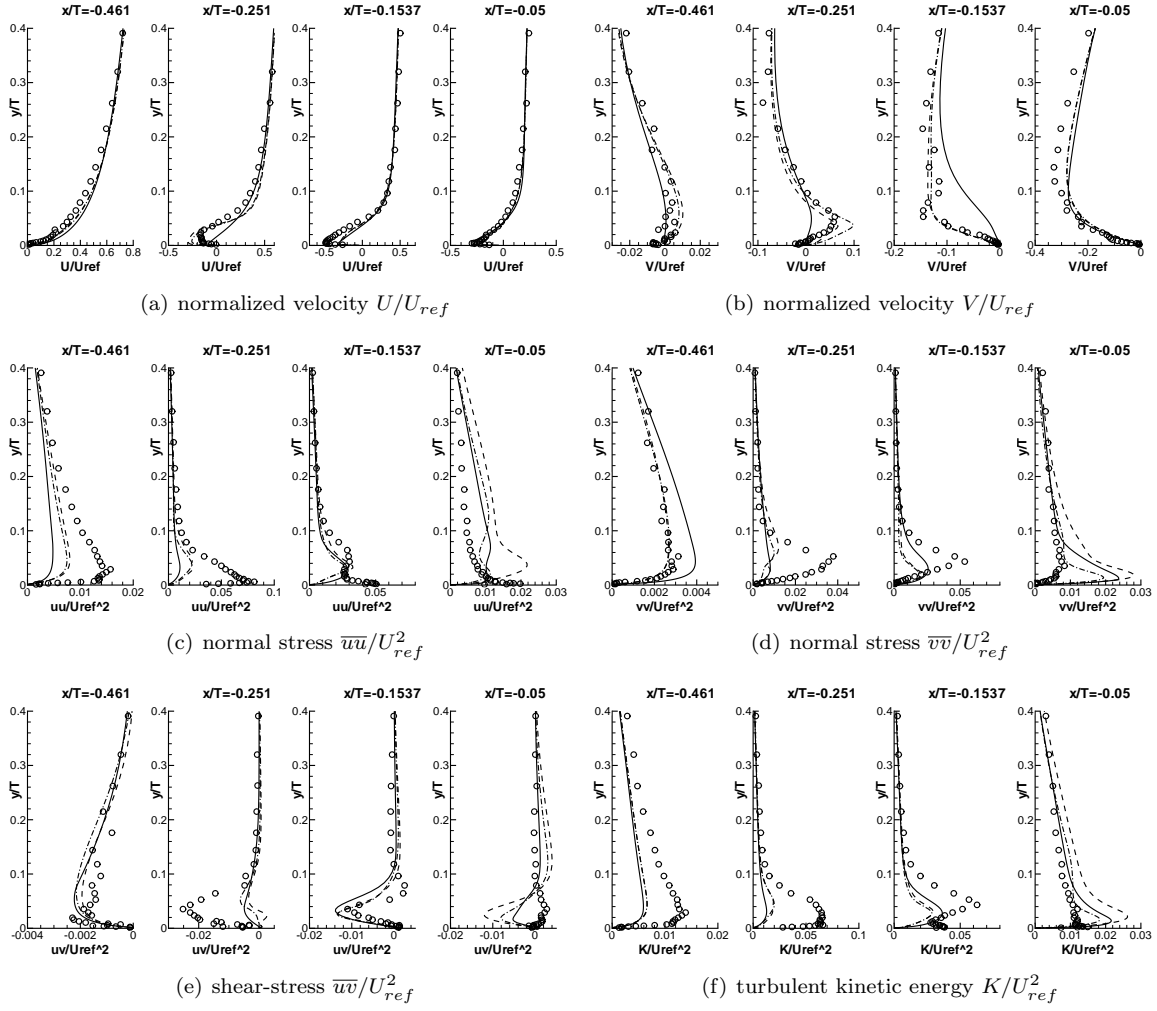
American Institute of Aeronautics and Astronautics

(a) normalized velocity U/U_{ref} (b) normalized velocity V/U_{ref}

(c) normal stress $\overline{uu}/U_{ref}^2$ (d) normal stress $\overline{vv}/U_{ref}^2$

(e) shear-stress $\overline{uv}/U_{ref}^2$ (f) turbulent kinetic energy K/U_{ref}^2

Figure 4. Symmetry plane at $z/T = 0$. ($\circ$) Experiment[19] , (—) Kω-SST, ($- \cdot -$) 2D-EASM, (- - -) 3D-EASM.

that both 2D/3D-EASM formulations are again clearly superior compared to the Kω-SST in predicting the mean flow velocity field. For the streamwise velocity component, both EASM closures predict the correct shape and the distortion of the velocity profile, while the Kω-SST does not capture this distortion. Both nonlinear EASM formulations predict the extent and magnitude of the transverse circulation in very good agreement with experimental data. The Kω-SST model under predicts the magnitude of the transverse circulation in this plane, which is consistent with under predicted reverse flow intensity in the symmetry plane. The difference between the 2D and 3D EASM formulations is again found to be negligible, indicating the higher order coupling terms in the constitutive relations of the 3D-EASM are not contributing significantly to the mean flow characteristics at this station.

The predictions of the turbulence quantities at $x/T = 0.76$ again shows a more pronounced departure from experimental data, indicating that the quality of the predictions of the Reynolds stress components is not directly linked to the quality of the predictions of the mean velocity field. Generally speaking, the non-linear EASM formulations predict the stress components in better agreement with the experiment than the linear Kω-SST model does. The improvements are associated with the ability of the EASM models to predict extra anisotropy in addition to the anisotropy induced by the mean flow or strain-rate tensor S_{ij}. Even though the correct trend of the turbulence quantities is mainly reproduced, deficiencies exists in predicting the correct magnitude close to the wall. As discussed for the planar channel flow, this feature could be an artefact of the lack of adequate modifications of the quasi-homogeneous pressure strain model and the high-Reynolds number form of the transport equations for the turbulence quantities.
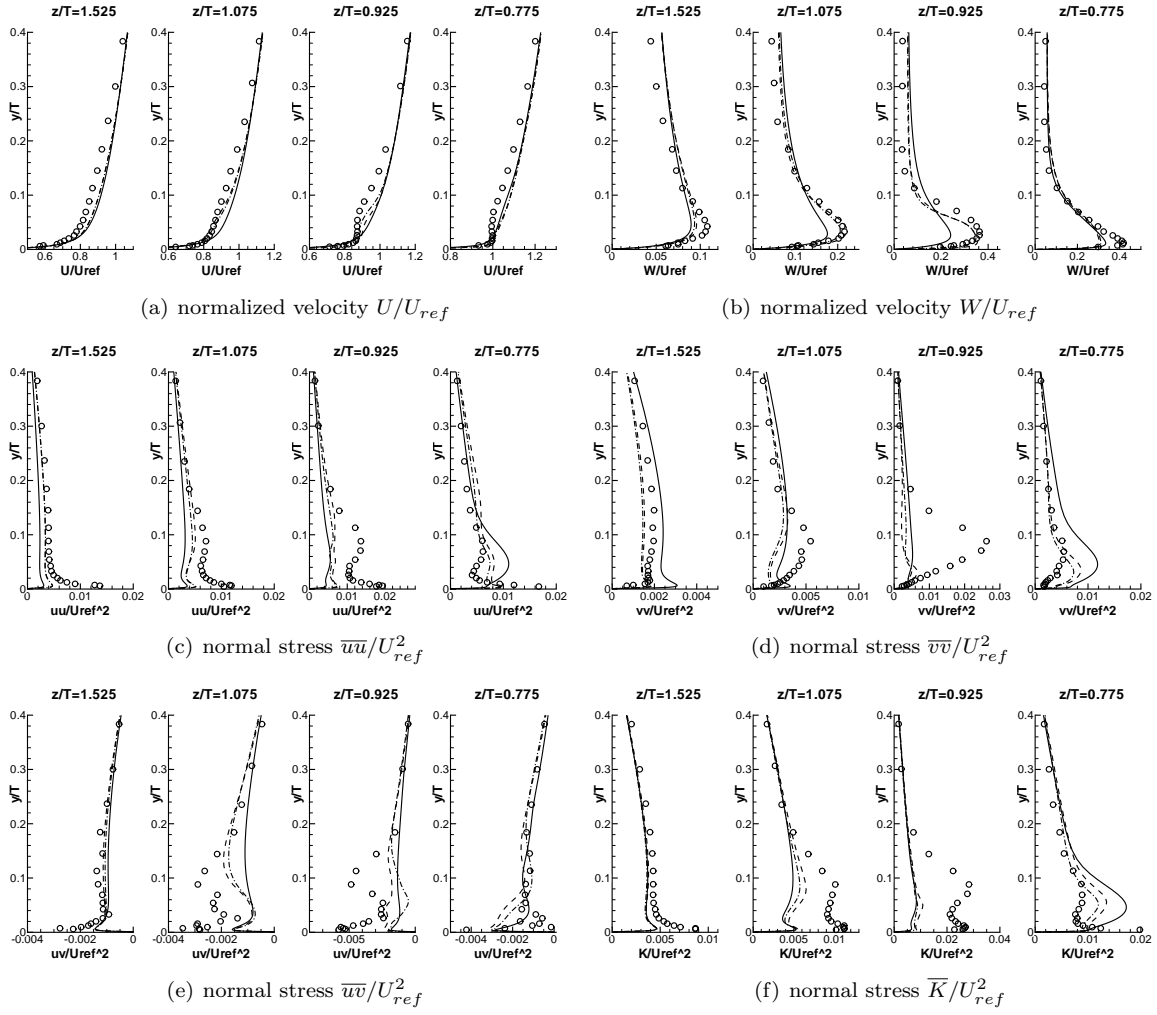
American Institute of Aeronautics and Astronautics

Figure 5. Cross section at $x/T = 0.76$. (○) Experiment[19] , (——) Kω-SST, (— · —) EASM 2D, (- - -) EASM 3D.

C. Flow around a three-dimensional hill

The test case considered next consists of a three-dimensional axisymmetric hill which is approached by a turbulent boundary layer with a thickness of half the hill height $\delta = 0.5H$, as shown in figure 6. The Reynolds number is $Re_H = 1.3 \cdot 10^5$, based on the hill height $H = 0.078m$ and the maximum channel centerline velocity at the inlet $U_{ref} = 27.5m/s$. This configuration was the subject in the 11th and 12th ERCOFTAC Workshop on Refined Turbulence Modelling and has proven to be a particularly challenging test case for any RANS turbulence model. Detailed experimental data are provided by Simpson *et al.*[22] and highly resolved LES data[23] are also available for comparison. The main difficulties are associated with the prediction of the separation from a smooth three-dimensional surface, a recirculation and recovery region, and complex three-dimensional vortical structures forming on the leeward side of the hill.

The grid used for the simulations consists of 2.2 million cells with a first average grid spacing adjacent to walls of $y^+ \approx 0.5$ and a maximum value of $y^+ \approx 0.8$. The boundary conditions are zero normal gradient boundary conditions for the outflow, zero-stress boundary conditions for both side walls, and no-slip boundary conditions for the upper and lower channel wall. Unfortunately, no measurements where taken upstream of the hill which could be used as inflow boundary conditions. Instead, measurements where taken at the location of the center of the hill when the hill was removed from the tunnel. In order to specify appropriate inflow conditions, a separate channel flow simulation is performed and the profiles are matched to the experimental data when the hill is not in place. The inflow condition for the turbulence quantities and the velocity profile are then obtained by using the the data at $x/H = 6$ upstream of the matching location.
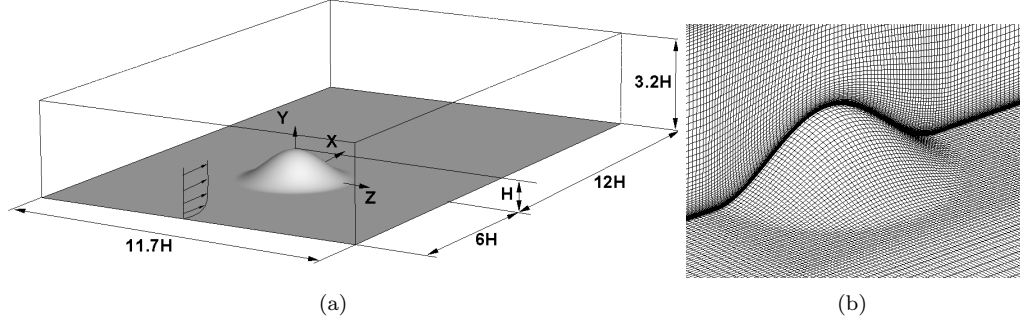
American Institute of Aeronautics and Astronautics

Figure 6. Geometry and computational grid for the axisymmetric hill.

Figure 7 shows normalized profiles for the velocity components U/U_{ref}, V/U_{ref}, W/U_{ref}, turbulent kinetic energy K/U_{ref}^2, the components of the Reynolds stress tensor $\overline{uu}/U_{ref}^2$, $\overline{vv}/U_{ref}^2$, $\overline{ww}/U_{ref}^2$, and $\overline{uv}/U_{ref}^2$ at four different stations inside the measurement plane $x/H = 3.63$ downstream of the hill. The profiles are support by figure 8 which shows contour plots of the streamwise velocity and streamlines in the measurement plane.

As in previous RANS studies for this case,[24] the components of the velocity profile in the central region of the wake are poorly predicted by all closures studied here. All models show a similar, significant under-prediction of streamwise velocity in the region $y/H < 0.5$, indicating a far too slow recovery of the flow. In addition, the contour plots reveal a considerable departure of the predicted topology of the streamwise flow component. The failure of the RANS models becomes clearer by inspecting the wall-normal and spanwise velocity components. All RANS models predict a strong upwash of the wall-normal velocity and a transverse motion towards the central region of the wake. This is confirmed by figure 8, which reveals the presence of two large counter rotating vortices in the wake. Both experiment and LES show not only the exact opposite behaviour, they also show a significant departure in the flow topology. At the center of the wake, a downwash exists which promotes the fast recovery observed in the experiments and the transverse motion is directed away from the central plane. As a consequence, the RANS models studied here, and elsewhere,[24] return an unphysically large separation region on the leeward side of the hill, whereas a very thin separation zone is present in the experiment.

For the region $y/H > 0.5$, the predictions of the Kω-SST compare favourably to the predictions of both EASM formulations. Figure 8 reveals that the Kω-SST model predicts delayed separation compared to both EASM formulations. This results in a vortex pair which is predicted to be closer to the lower wall with a less intense transverse motion. Since the extent of the vortex is smaller, the distortion of the streamwise velocity is limited to a smaller region close to the wall. At the measurement stations further away from the center plane, the difference in streamwise velocity between the models vanishes. From the above, it becomes apparent, that the RANS models completely fail in predicting the mechanisms leading to the formation of the complex, vortical structure on the leeward side of the hill. This might be linked to an erroneous prediction of the separation process. The separation in the LES simulations is observed to be strongly unsteady in nature and shows great variation in both space and time due to vortex shedding from the hill surface and complex interaction with the wake, as discussed in García-Villalba *et al.*[23]

Even though it seems unlikely that the highly unsteady, three-dimensional separation process can be predicted with sufficient accuracy within the RANS framework, the three-dimensional nature of the flow allows for an investigation of potential differences between 2D and 3D-EASM formulations and models based on a linear stress-strain relationship.

In the central region of the wake both EASM formulations tend to considerably over predict the magnitude of the Reynolds stress components compared to the Kω-SST model. The Kω-SST predicts much lower levels of turbulence intensity which is in better agreement with the experimental data. The difference is not that surprising since the predicted mean velocity field also shows a considerable departure in the outer region. It is noted here, that the experimental data and the LES data[23] show inconsistent behaviour for the region $y/H > 0.5$. The LES simulation consistently shows a smaller magnitude of the predicted stress components as well as a slightly different shape of the velocity profile in the outer region. The predicted
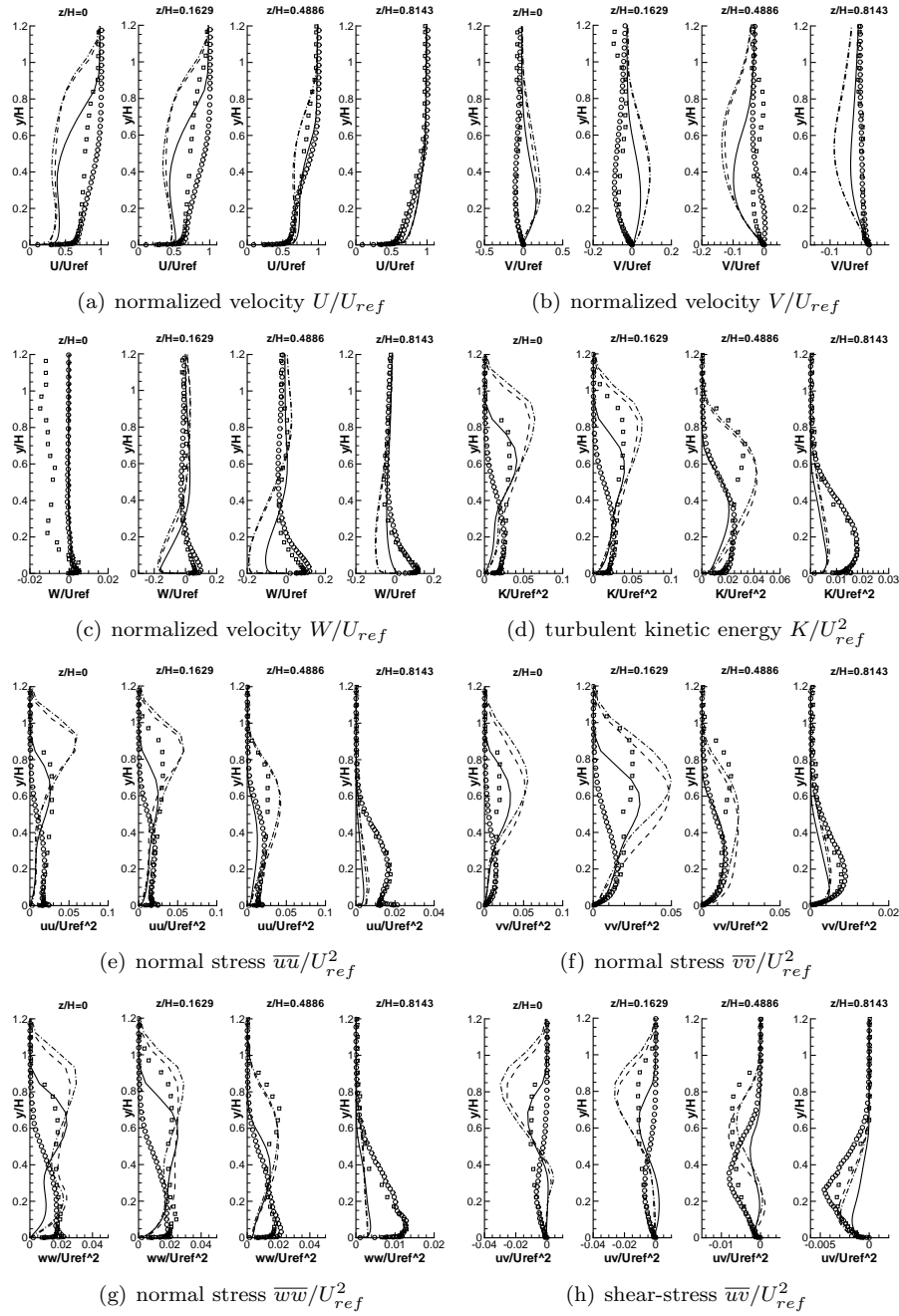
American Institute of Aeronautics and Astronautics

(a) normalized velocity U/U_{ref} (b) normalized velocity V/U_{ref}

(c) normalized velocity W/U_{ref} (d) turbulent kinetic energy K/U_{ref}^2

(e) normal stress $\overline{uu}/U_{ref}^2$ (f) normal stress $\overline{vv}/U_{ref}^2$

(g) normal stress $\overline{ww}/U_{ref}^2$ (h) shear-stress $\overline{uv}/U_{ref}^2$

Figure 7. Measurement plane at $x/H = 3.63$. ($\circ$) LES[23] , ($\square$) Experiment[22] , (——) Kω-SST, ($-\cdot-$) 2D-EASM, ($---$) 3D-EASM.

stress components in the inner region $y/H < 0.5$ are in slightly better agreement than in the outer part, and the models investigated return somewhat more consistent results. However, significant amplitude errors are again obtained for various quantities and peaks near the wall are not captured.

Considering the difference in the predictions between the 2D and 3D-EASM, it can be noted, that the mean velocity profiles are equally predicted by both EASM versions. Differences seem to be slightly more pronounced in the central region of the wake than in the region further away from the central plane, where the difference is indeed vanishing. Both EASM formulations also predict most turbulence quantities in close agreement. From the results above, the use of the more expensive three-dimensional EASM formulation seems not necessary since the overall difference in the predictions is negligible.
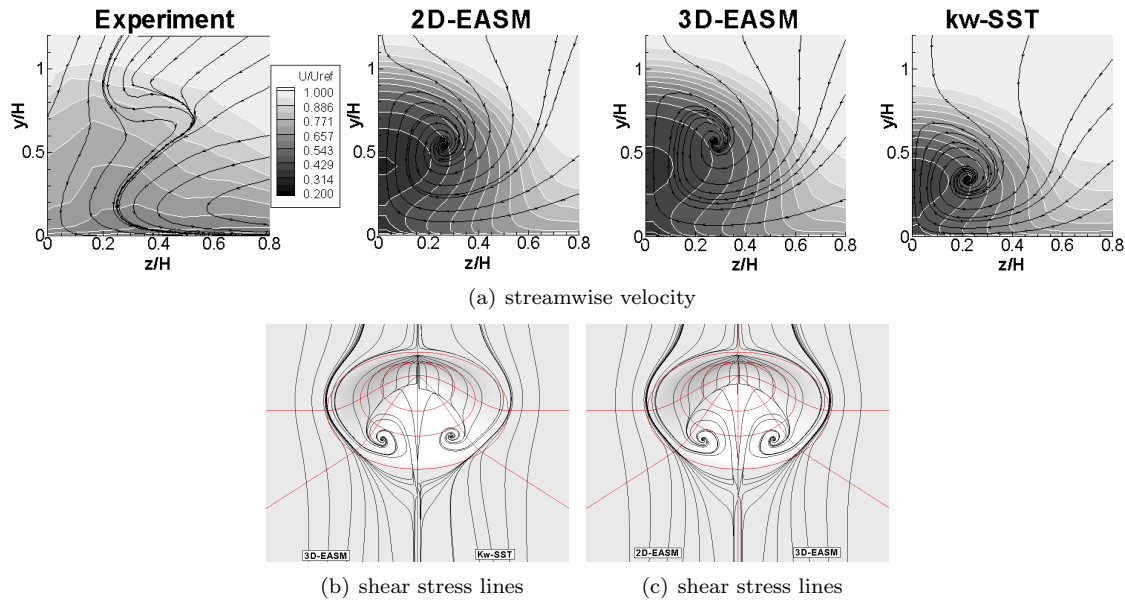
(a) streamwise velocity

(b) shear stress lines

(c) shear stress lines

Figure 8. Contour plot at $x/H = 3.63$ downstream of the hill

V.   Conclusion

In this paper, the predictive capabilities of two and three-dimensional formulations of Explicit-Algebraic-Stress models to predict complex three-dimensional flows was investigated. The focus of this study was placed on investigating the necessity and importance of the extra nonlinear coupling terms that appear in the integrity basis of Explicit-Algebraic-Stress model which are derived for general three-dimensional mean flows. The simulations for the wing-body junction clearly demonstrate the improved performance of both 2D and 3D-EASM models compared to traditional turbulence models which are based on a linear stress-strain relationship. The most significant improvements were observed in predicting the mean velocity field in good agreement with experimental data. The ability of both EASM formulations to resolve stress-anisotropy is reflected in improved predictions of the components of the Reynolds stress tensor. The predictions of the turbulence quantities were not entirely satisfactory, particularly in terms of predicting the correct magnitude of the turbulent intensity. Also, the near wall peaks in the turbulent kinetic energy and normal stress components were generally not captured, probably due to the lack of adequate near wall modifications of both the EASM models and the Kω-SST. The predictions of the wall normal fluctuations and the strong damping close to the wall were found to be severely in error in some regions of the flow field. It is suggested that the inclusion of the correct damping mechanisms would require the information from at least one more transport equation of the wall normal fluctuations.

For the axisymmetric hill case none of the models investigated here was able to reproduce the correct flow topology on the leeward side of the hill. Since even the most sophisticated RANS model predicts massive separation and far too slow recovery of the wake, this test case clearly demonstrates the lack of fidelity of the RANS approach to cope with flows departing from the conditions they have been designed and calibrated for.

Both test cases also revealed that the two and three-dimensional formulation of the EASM models predicted equivalent or very similar results. Since the three-dimensional EASM formulations has not been found to give improved or significantly different predictions, the considerable additional numerical expense compared to the two-dimensional formulation does not seem to be justified for the test cases used in this study. However, although the test cases considered here include a range of different complex, three-dimensional flow features, the conclusions drawn here cannot necessarily be extend to other arbitrary complex, three-dimensional flows.

American Institute of Aeronautics and Astronautics

Acknowledgments

References

[1] Rodi, W., "A new algebraic relation for calculating the Reynolds stresses," *Zeitschrift für angewandte Mathematik und Mechanik*, Vol. 56, 1976.

[2] Rodi, W., *The prediction of free turbulent boundary layers by use of a two-equation model of turbulence*, Ph.D. thesis, University of London, 1972.

[3] Pope, S. B., "A more general effective-viscosity hypothesis," *Journal of Fluid Mechanics*, Vol. 72, Part 2, 1975, pp. 331–340.

[4] Gatski, T. B. and Speziale, C. G., "On explicit algebraic stress models for complex turbulent flows," *Journal of Fluid Mechanics*, Vol. 254, 1993, pp. 59–78.

[5] Taulbee, S. B., "Stress relation for three-dimensional turbulent flows," *Physics of Fluids*, Vol. 6, Issue 3, 1994, pp. 1399–4101.

[6] Wallin, S. and Johansen, A. V., "An explicit algebraic Reynolds stress model for incompressible and compressible turbulent flows," *Journal of Fluid Mechanics*, Vol. 403, 2000, pp. 89–132.

[7] Girimaji, S. S., "Fully-Explicit and Self-Consistent Algebraic Reynolds Stress Model," *Theoretical and Computational Fluid Dynamics*, Vol. 8, No 6, 1996, pp. 387–402.

[8] Launder, B. E., Reece, G. J., and Rodi, W., "Progress in the development of a Reynolds-stress turbulence closure," *Journal of Fluid Mechanics*, Vol. 68, part 3, 1975, pp. 537–566.

[9] Speziale, C. G., Sarkar, S., and Gatski, T. B., "Modelling the pressure-strain correlation of turbulence: an invariant dynamical systems approach," *Journal of Fluid Mechanics*, Vol. 227, 1991, pp. 245–272.

[10] Wilcox, D. C., "Comparison of Two-Equation Turbulence Models for Boundary Layers with Pressure Gradient," *AIAA Journal*, Vol. 31, No. 8, 1993, pp. 1414–1421.

[11] Yorke, C. P. and Coleman, G. N., "Assessment of common turbulence models for an indealized adverse pressure gradient flow," *European Journal of Mechanics B/Fluids*, Vol. 23, 2004, pp. 319–337.

[12] Sciberras, M. A. and Coleman, G. N., "Testing of Reynolds-stress-transport closure by comparison with DNS for an idealized adverse-pressure gradient boundary layer," *European Journal of Mechanics B/Fluids*, Vol. 26, 2007, pp. 551–582.

[13] Menter, F. R., "Two-Equation Eddy-Viscosity Turbulence Models for Engineering applications," *AIAA Journal*, Vol. 32, No. 8, 1994, pp. 1598–1604.

[14] Hellsten, A., *New Two-Equation Turbulence Model for Aerodynamic Applications*, Ph.D. thesis, Helsinki University of Technology, Laboratory of Aerodynamics, 2004.

[15] "OpenCFD Ltd - OpenFOAM: http://www.opencfd.co.uk/," .

[16] Moser, R. D., Kim, J., and Mansour, N. N., "Direct numerical simulation of a turbulent channel flow up to $Re_\tau = 590$," *Physics of Fluids*, Vol. 11, Issue 4, 1999.

[17] Apsley, D. D. and Leschziner, M. A., "Investigation of Advanced Turbulence Models for the Flow in a Generic Wing-Body Junction," *Flow, Turbulence and Combustion*, Vol. 67, 2001, pp. 25–55.

[18] Simpson, R. L., "Junction Flows," *Annual Review of Fluid Mechanics*, Vol. 33, 2001, pp. 415–443.

[19] Fleming, J. L., Simpson, R. L., and Devenport, W. J., "An Experimental Study of a Turbulent Wing-Body Junction and Wake Flow," *Experiments in Fluids*, Vol. 14, 1993, pp. 366–378.

[20] Durbin, P. A., "Near-Wall Turbulence Closure Modeling Without Damping Functions," *Theoretical and Computational Fluid Dynamics*, Vol. 3, 1991, pp. 1–13.

[21] Parneix, S., Durbin, P. A., and Behnia, M., "Computation of 3D Turbulent Boundary Layers Using the V2F Model," *Flow, Turbulence and Combustion*, Vol. 60, 1998, pp. 19–46.

[22] Simpson, R. L., Long, C. H., and Byun, G., "Study of vortical separation from an axisymmetric hill," *International Journal of Heat and Fluid Flow*, Vol. 23, 2002, pp. 582–591.

[23] Garcia-Villalba, M., Li, N., Rodi, W., and Leschziner, M. A., "Large-Eddy simulation of separated flow over a three-dimensional axisymmetric hill," *Journal of Fluid Mechanics*, Vol. 627, 2009, pp. 55–96.

[24] Wang, C., Jang, Y. J., and Leschziner, M. A., "Modelling two-and three-dimensional separation form curved surfaces with anisotropy resolving turbulence closures," *International Journal of Heat and Fluid Flow*, Vol. 25, 2004, pp. 449–512.